RSC Advances

ROYAL SOCIETY OF CHEMISTRY

www.rsc.org/advances

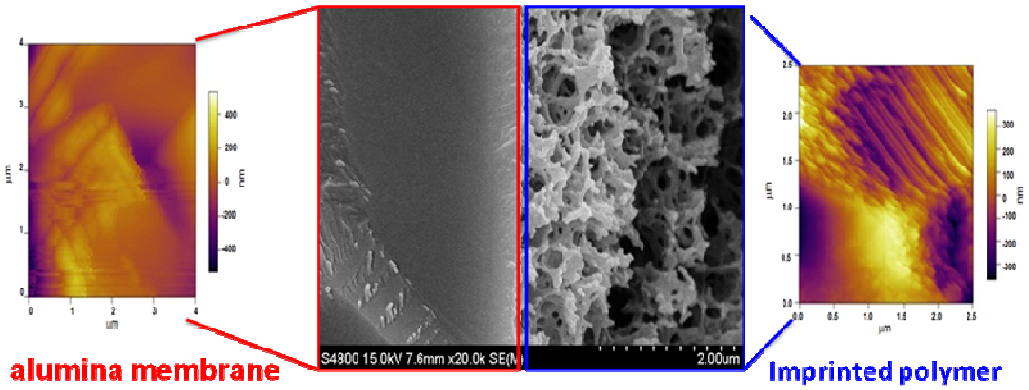

Highly selective composite imprinted alumina membrane (CIAM) for gentisic acid (GA) was successfully prepared via non-hydrolytic sol–gel method to targed separation.

Introduction of ordered porous polymer network into ceramic alumina membrane via non-hydrolytic sol–gel methodology for targeted dynamic separation

Minjia Meng[a], Yan Liu[a], Min Zhang[a], Yonghai Feng[b], Yongsheng Yan[a]*

[a]School of Chemistry and Chemical Engineering, Jiangsu University, Zhenjiang 212013, China

[b]School of Material Science and Engineering, Jiangsu University, Zhenjiang 212013, China

Abstract

Highly selective composite imprinted alumina membrane (CIAM) for gentisic acid (GA) was successfully synthesized by the nonhydrolytic sol–gel (NHSG) method with room temperature ionic liquid (RTIL) as pore template. The carboxylic acid was used as both the functional monomer and the catalyst to form alumina membrane-based porous imprinted polymer layer. The adsorption capacities, fluxes and permeation selectivities of varied CIAM suggested that cinnamic acid (CA) was the promising functional monomer for preparing CIAM to separate GA from salicylic acid (SA) and the incorporation of RTIL improved the selectivity of GA over CIAM. The amount of porous imprinted polymer layer on CIAM significantly affected the separation of GA from SA over CIAM. A three-level Box–Behnken experimental design with three factors combining the response surface modeling was used to optimize dynamic separation process. The experimental data were well fitted to a second-order polynomial equation using multiple regression analysis. The optimal conditions for the separation of GA from SA were as follows: the GA concentration of 0.0325 mmol L^{-1}, the temperature of 15.0 ^{o}C and the flow rate of 1.0 mL min^{-1}. Under these conditions, the experimental separation factor was 13.26 ± 0.87%, which was close to the predicted separation factor.

Keywords: Gentisic acid, Composite imprinted alumina membrane, Selectivity, Room temperature ionic liquid, Box–Behnken experimental design

1 Introduction

Salicylic acid (SA) has been used worldwide in many industrial applications, including ointment, liquid, cream or plaster, for the treatment of acne, psoriasis, warts, ichthyosis and other hyperkeratotic disorders.[1] It is also used as raw material for the production of aspirin.[2] Commercial SA is usually produced along with a mixture of isomers and analogues, which are usually toxicant and harmful to lives. From among these, gentisic acid (GA) is usually generated as an SA analogue in the production of SA. The separation of GA from SA is hardly achieved by conventional separation methods due to their similar structures. Therefore, it is necessary to develop efficient methods to separate GA from SA for ensuring the high purity of SA.

Membrane separation is an emerging technology with advantages of low energy costs, low environmental impact, and possible integrated processes with selective removal of certain components.[3–4] However, usual commercial membranes do not allow the selective separation of analogues,[5] implying that the separation of analogues is hard to achieve by using the commercial membranes. Therefore, methods of preparing composite membranes with controlled specificity for selective separation of analogues have attracted considerable attentions.

Molecular imprinting is a good method for preparing polymers with specific recognition for template molecule,[6] which are called the molecularly imprinted polymers (MIPs) and widely used in chromatography,[7] solid phase extraction,[8] chiral separations,[9,10] synthesis and catalysis,[11,12] enzyme mimics[13,14] and so on. Using the molecular imprinting technique to prepare molecularly imprinted membrane has

attracted great attention from researchers because it suggested an innovative and facile way to synthesize composite membrane for selective separation of analogues. Yoh-ichi Tagawa et al.[15] have investigated polymeric membranes in detail for chiral separation of pharmaceuticals and chemicals. The pioneer work demonstrated that the use of imprinting membranes is of great importance for chiral separation. However, the recognition sites and adsorption capacity of the polymeric membranes were relative low due to the shortcomings of the preparation method. In these cases, improving the recognition sites and adsorption capacity of the imprinting membranes for selective separation of analogues are still a challenge.

Recently, the sol–gel imprinting method has been thought to an alternative method for preparing MIPs, through which organic/inorganic materials with unique structure and highly selective recognition could be formed.[16–18] This methodology is based on the non-hydrolytic sol–gel (NHSG) process and the molecular imprinting technique. The NHSG technique does not require aging and drying steps at high temperatures. Since little or no water is evolved in the synthesis, the cracking and shrinking of the gelatin by the hydrolytic sol–gel method are avoided. Thus, NHSG process can subtly retain binding sites and increase the selectivity of the imprinted material. [19]

Room temperature ionic liquid (RTIL) as the interesting solvents has been widely used in organic synthesis, catalysis, electrochemical purposes, etc.[20–22] RTIL is also a promising pore template in the sol–gel reaction,[23–25] which accelerated the synthesis and improved the selectivity of imprinted polymers**.**

In the present work, a novel way was developed for selective separation of GA

from SA. Three kinds of composite imprinted alumina membranes (CIAM) for GA were prepared by NHSG imprinted method with RTIL used as the pore template. The as-prepared CIAM were characterized by Fourier transform infrared spectrometer (FT-IR), transmission electron microscope (SEM) and atomic force microscope (AFM) techniques. The as-prepared CIAM showed highly selective recognition of GA. A three-level Box-Behnken experimental design with three factors combining the response surface modeling was used for Optimization of dynamic separation of GA from SA.

2 Experimental

2.1. Materials

Al_2O_3 microporous membranes with a nominal pore size *d*p=4 μm and a thickness of 2 mm, were purchased from Hefei Great Wall Xinyuan film Technology Co., Ltd. Salicylic acid (SA), gentisic acid (GA), methacrylic acid (MAA), acrylic acid (AA), cinnamic acid (CA), acetonitrile, methacryloxypropyltrimethoxysilane (MPS), 2,2′ -azobis(2-isobutyronitrile) (AIBN), 1-methylimidazole, chlorobutane and hexafluorophosphoric acid were all purchased from Sinopharm Chemical Reagent (Shanghai, China). All other chemicals used were of analytical grade and obtained commercially. Ultra pure water used throughout the experiments was obtained from laboratory purification system.

2.2. Synthesis of Composite Imprinted Alumina Membrane (CIAM)

2.2.1. Preparation of ionic liquid (RTIL)

1-Butyl-3-methylimidazolium chloride ([BMIM]Cl) was prepared according to the

report by Rogers et al.[26] In the typical experiment, 61.58 g of 1-methylimidazole (0.75 mol) and 69.43 g of chlorobutane (0.75 mol) were added in a 250 mL of round-bottomed flask fitted with a reflux condenser by heating and stirring at 70 ^{o}C for 72 h. The resulting viscous liquid ([BMIM)Cl) was allowed to cool to room temperature and then was washed three times with 200 mL portions of ethyl acetate. After the last washing, the remaining ethyl acetate was removed by heating to 70 ^{o}C under vacuum. To prepare the ionic liquid, hexafluorophosphoric acid (94.88 g, 0.65 mol) was added (slowly to prevent the temperature from rising significantly) to a mixture of [BMIM]Cl (87.34 g, 1 mol) in 500 mL of water. After stirring for 12 h, the upper acidic aqueous layer was decanted and the lower ionic liquid portion was washed with water until the washings were no longer acidic. The ionic liquid ([BMIM]PF_6) was then heated under vacuum at 70 ^{o}C to remove any excess water.

2.2.2. Preparation of CIAM

In this research, varied composite imprinted alumina membranes (CIAM) were synthesized. The compositions are presented in Table 1.

At first, the surfaces of Al_2O_3 microporous ceramic membranes were boiled in 30% hydrogen peroxide for 30 min to introduce -OH groups on the surface for further modification. They were then boiled in deionized water for 15 min to clean the surface and then dried under nitrogen condition.

Secondly, GA (1.0 mmol), functional monomer (MAA, AA or CA) (4.0 mmol) and acetonitrile (12.0 mL) were mixed in a conical flask for 4 h in order to obtain the self-assembled composites with GA. Then MPS, [BMIM]PF_6 and AIBN were added

to the solution forming the prepolymerization mixture (see Table 1). Then several pretreated Al_2O_3 microporous ceramic membranes were immersed into the prepolymerization solution and the prepolymerization mixture was submerged into a 54 ^oC water bath for 12h.

Finally, the imprinted membranes were moved out of the water bath and immediately flushed with several volumes of mixed solvents of methanol and acetic acid (9:1, V/V) by ultrasound to remove the unreacted reagents, the RTIL and the imprinting molecule GA. Then the composite imprinted alumina membrane (CIAM) for GA was obtained by rinsing with methanol and drying and the specific recognition sites for GA were left after removing the template (Scheme 1).

The composite non-imprinted alumina membrane (CNAM) was prepared in parallel without addition of GA.

2.3. Characterization

The prepared RTIL was characterized by FT-IR spectra (Nicolet NEXUS-470, USA). The morphologies of surface and cross-sectional structures of the samples were obtained by scanning electron microscopy (SEM, S-4800). Topographical atomic force microscope (AFM) images of unmodified and imprinted alumina membranes were made in tapping mode (Veeco Instruments Inc.) with an atomic force microscope (MicroNano AFM-III).

2.4. Batch selective rebinding assay

A piece of composite imprinted membrane (or a piece of blank membrane) was added into conical flask, each of which contained 20 mL solution of GA and SA,

respectively. Then it was shocked at 25 ^{o}C for 4 h in a water bath oscillator. Then, substrate concentration (GA and SA) in the solution was analyzed using UV spectrophotometry and the binding amount of each substrate can be calculated by the following equation:

$$q_e = \frac{(C_0 - C_e)V}{W} \quad (1)$$

Where C_0 (mmol L^{-1}) and C_e (mmol L^{-1}) represent the concentration of substrates measured at an initial and saturated binding time. V (L) and W (g) are the volume of the solution and the weight of the imprinted membrane, respectively.

The distribution coefficients (K_d), selectivity coefficients (α) of GA with respect to SA can be obtained according to the following equation:

$$K_d = \frac{q_e}{C_e} \quad (2)$$

K_d (mL g^{-1}) represents the distribution coefficient, q_e (μmol g^{-1}) and C_e (μmol L^{-1}) are the equilibrium binding amount and the equilibrium concentration of the adsorbate, respectively. The selectivity coefficient α can be obtained according to the following equation:

$$\alpha = \frac{K_{d(GA)}}{K_{dj}} \quad (3)$$

Where, K_{dj} represents the distribution coefficient of competition species.

2.5. Membrane flux experiment

The aqueous solution containing 0.65 mmol L^{-1} GA was prepared as feed solution, and the composite imprinted membrane and blank membrane were fitted on the ultrafiltration cell with 25 mm diameter (UF-8010, Amicon). The feed solution was permeated through the membrane (operation pressure: 0.15 MPa), and the flux of the

feed solution passing different membranes were calculated by the following equation:

$$F = \frac{V}{st} \quad (4)$$

Where V is volume of permeate solution (mL), t and s represent operation time (min) and effective area of membrane (cm^2), respectively.

2.6. Permeation Experiments

The permeate experiments were carried out using the mixture solutions with varied concentrations of GA and SA as the feed solution. The permeate experiments were performed in a two-compartment cell (effective membrane area = 1.5 cm^2; capacity = 150 mL × 2). The membrane was fixed between the compartments. Then, the mixture solution of GA and SA (100 mL) in methanol was placed in the left-hand side chamber, while 100 mL methanol was placed in the right-hand side chamber. The permeation experiments were done at 25 ^oC. Finally the concentration of both GA and SA in the permeate solution was determined by a UV system. The amounts of the substrate that permeated the membranes were determined by a UV system. The flux J (mmol cm^{-2} s^{-1}), permeability coefficient P (cm^2 s^{-1}) and separation factor (perm-selectivity) $\alpha_{ASA/SA}$ can be calculated by the following equations:

$$J_i = \frac{\Delta C_i V}{\Delta t A} \qquad i=\text{SA, GA} \quad (5)$$

$$P = \frac{J_i d}{(C_{Fi} - C_{Ri})} \qquad i=\text{SA, GA} \quad (6)$$

$$\alpha_{SA/GA} = \frac{P_{SA}}{P_{GA}} \quad (7)$$

where $\Delta C_i/\Delta t$ is the concentration change rate of the receiving solution which can be

obtained by calculating the slope value of the diffused analyte concentration–time curve, V is the volume of solution, A is the effective membrane area (cm^{-2}), d is the membrane thickness and ($C_{Fi}-C_{Ri}$) is the concentration difference between feeding and receiving chambers.

2.7 Optimization of dynamic separation of GA from SA

In order to be able to predict and control the dynamic separation of GA from ASA, optimization studies should be conducted. The response surface methodology (RSM), introduced by Box and Wilson, which is a collection of mathematical and statistical techniques whose purpose is to analyze, by an empirical model, problems as the one posed.[27] RSM includes much more model fitting and analysis of them. The relation between variables and response is theoretically described by a function that is the underlying physical mechanism to the problem under study. Second-order model are usually studied for fitting response surfaces.

In the study, Box–Behnken design (BBD) model of RSM was used for the determination of optimum levels of the processing variables for the parameters studied.[28] A 3-factor-3-level BBD was applied to design the experimental conditions using Design-Expert software involving three factors, the concentration of GA (A), temperature (B) and flow rate (C) of separation process, which were chosen as independent variables. The selected responses for analysis were separation factor (β) based on equations (8). The levels of the variable factors in the experiment and the experimental design with the parameters are given in Table 2.

$$\beta = \frac{C_{eSA}(C_{fGA} - C_{eGA})}{C_{eGA}(C_{fSA} - C_{eSA})} \quad (8)$$

where β is the selective separation factor during the dynamic separation process, C_{fGA} and C_{fSA} are the initial concentration of GA and SA in the feeding solutions (mmol L^{-1}), respectively, C_{eGA} and C_{eSA} are the effluent concentration of GA and SA from the column (mmol L^{-1}), respectively.

The mathematical relationship between responses (Y) and the three significant independent variables (A, B, and C) were usually described by estimating coefficients of the following second-order polynomial model based on experimental data.[28]

$$Y= \beta_0 +\beta_1 A+\beta_2 B+\beta_3 C+\beta_{11} A^2+\beta_{22} B^2+\beta_{33} C^2+\beta_{12} AB+\beta_{13} AC+\beta_{23} BC$$

where, Y is the response function, β_0 is an constant, β_1, β_2 and β_3 are the coefficients of the linear, β_{11}, β_{22}, and β_{33} are quadratic coefficients, β_{12}, β_{13} and β_{23} are the interaction coefficients between the three factors.

A multiple regression analysis was done to obtain the coefficients and the equation could be used to estimate the response. A total of 17 experiments were needed to estimate the full model. All the experimental data were statistically analyzed by the software package Design-Expert 8.0.5b. p-values of less than 0.05 were considered to be statistically significant.

3. Results and discussion

3.1 UV study

The interaction between the functional monomers (MAA, AA or CA) and GA was studied by UV spectroscopic analysis due to that the functional monomers strongly interact with the template and form stable host-guest complexes prior to polymerization .[29] The results were shown in Fig. 1.

As shown in Fig. 1a-c, it was clearly observed that the maximum absorbance at 215 nm of the mixture solutions decreased with the increase in the functional monomer concentration. The maximum absorption wavelength showed variable changes of redshift, showing that the interaction between functional monomer and GA was getting stronger when increased the concentration of functional monomer. The changes of the maximum absorbance for any functional monomer became smaller when the molar ratio of the template and functional monomer was greater than 1:4. It demonstrated that 1:4 was the optimal molar ratio chosen for the synthesis of IAM Since too large amount of functional monomers may lead to their own association and increase nonselective binding sites. Among the three functional monomers, CA had more obvious changes, indicating stronger interaction between CA and GA.

3.2. FTIR spectrum

To ascertain the successful preparation of the ionic liquid, FT-IR spectra (Fig. 2) were obtained for [BMIM]Cl and [BMIM]PF_6. For [BMIM]Cl, the band around 3145 cm^{-1} and 2800-3000 cm^{-1} are, respectively, aromatic and aliphatic C–H stretches. The wide and strong adsorption band around 3421 cm^{-1} could be ascribed to stretching vibrations of O-H of water which absorbed by [BMIM]Cl for its hydrophily. While no peak was found around 3421 cm^{-1}, indicating that the ion liquid ([BMIM]PF_6) is ill-suited to absorb water. Compared with [BMIM]Cl, a characteristic feature of [BMIM]PF_6 was the band around 833 cm^{-1} belonging to the adsorption peak of $[PF_6]^-$. It suggested that the ionic liquid was successfully synthetized.

3.3. Characterization

The surface microstructure (two and three-dimension) of Al_2O_3 ceramic membranes before and after imprinting polymerization was examined by AFM (Fig. 3). It can be observed that the surface topography (Fig. 3a) of Al_2O_3 ceramic membranes before modification visually shows a smooth surface. After imprinting polymerization, the surface topography of CA–CIAM exhibits orderly strip structure from Fig. 3c. Moreover, the topography of CA–CIAM greatly changes including the peak-to-valley height and roughness by comparison of the three-dimension images of Al_2O_3 ceramic membranes (Fig. 3b) and CA–CIAM (Fig. 3d). It is clear that the surface roughness of CA–CIAM become bigger after polymerization, while the topography of Al_2O_3 ceramic membranes appeared more homogeneous, which revealing that the well-distributed imprinted layer formed on the surface of Al_2O_3 ceramic membranes.

SEM analysis was used to further investigate the membrane surface and cross section microstructure. The microscopic structures of various prepared CIAM were studied by using SEM with gold-sputtered samples. As seen in Fig. 4a, Al_2O_3 ceramic membrane exhibited a more porous and smooth structure. Fig. 4b-d show that the surface of the MAA–CIAM, AA–CIAM and CA–CIAM were all mostly covered by a rough imprinted layer after the polymerization procedure, which can be clearly seen in the inset of the figure. Compared to the MAA–CIAM and AA–CIAM, it is evident that the formation of more regular pores is observed from the morphology of the imprinted layer on surface of CA–CIAM2.

Fig. 4d, e, f also presented the microphotographs of the surface of CA–CIAMs, which were prepared with pre-polymerization solutions with different amount of

crosslinker (shown in Table 1). Comparing with the differences in the morphology of CA–CIAM1, CA–CIAM2 and CA–CIAM3, it is found that CA–CIAM2 presents more regular pores than CA–CIAM1 and CA–CIAM3, which indicated the amount of crosslinker affected the structure of CIAM.

Fig. 5 presents the microphotographs of the cross section of the original membrane, CA–CIAM0, CA–CIAM2, CA–CNAM2. As can be seen from Fig. 5, there were significant difference in cross section morphology between nascent and imprinted membranes. The original Al_2O_3 ceramic membrane exhibited a smooth cross section structure. Fig. 5b, c and d show that the cross section of the CA–CIAM0, CA–CIAM2, CA–CNAM2 are all mostly covered by a thin imprinted layer on the base of Al_2O_3 ceramic membrane after the polymerization procedure. Compared with CA–CIAM0, the imprinted layer of CA–CIAM2 and CA–CNAM2 became much looser and formed more micropores, which would make the imprinted molecules access the binding sites exposed at the imprinted layer more easily. It was proved that the low vapor pressure of RTIL could assist in reducing the problem of gel shrinkage, and also act as pore templates in the sol–gel reaction.

Compared with imprinted membrane (CA–CIAM2), there were less differences between the morphology of imprinted and non-imprinted membrane (CA–CNAM2). Therefore, the distinct properties for imprinted and non-imprinted membrane could not entirely be attributed to the morphology difference, but to the imprinting effect.

All these changes of surface and cross section morphology of the Al_2O_3 ceramic membrane before and after polymerization indicated that the reaction between the

original ceramic membrane and pre-polymerization solution was indeed reliable.

3.4. Membrane flux studies

The relationship between operation time and flux of GA aqueous solution through different membranes was all recorded in Fig. 6. With the increase of operation time, the flux of membranes declined stablely. It was also observed from Fig. 6a that the water flux of GA aqueous solution was in an order of alumina membrane < CA–CIAM0 < CA–CNAM2 < CA–CIAM2. The higher water flux of CA–CIAM0, CA–CIAM2 and CA–CNAM2 than that of alumina membrane was probably due to lots of bingding sites on the outer surface and inner pores in the alumina membrane, which was beneficial for the accessibility and mass transport for GA. Additionally, CA–CIAM2 has a higher flux of GA compared with the non-imprinted membrane (CA–CNAM2), which might be ascribed to more selective cavities or adsorption sites obtained on the surface of CA–CIAM2 which promoted the permeation of GA.

The content of polymerization layer on the imprinted membrane was expected to strongly affect the flux of membranes. Fig. 6b shows the GA flux through the imprinted membranes (CA–CIAM1, CA–CIAM2 and CA–CIAM3) coated with various amounts of imprinted polymer.

The flux of GA decreased with the increase in the amount of coated polymer, especially for CA–CIAM3, the flux of which was lower than the original alumina membrane. It might be ascribed to that excessive polymer on the membrane will greatly reduce the porosity of membrane.

3.5. Batch adsorption studies of membrane

The adsorption capacity at equilibrium of varied CIAM and CNAM are shown in Fig. 7. The adsorption capacity of GA at equilibrium was *ca.* 100.4×10^{-3} μmol g^{-1}(AA), 125.7×10^{-3} μmol g^{-1} (MAA), 143.6×10^{-3} μmol g^{-1}(CA) for CIAM; and 62.56×10^{-3} μmol g^{-1} (AA), 78.45×10^{-3}μmol g^{-1}(MAA), 82.65×10^{-3}μmol g^{-1}(CA) for CNAM, respectively. It was found that the membrane (CIAM or CNAM) prepared with CA as the functional monomer had a higher adsorption capacity than the other two corresponding membranes. The results indicated that it was much easier for GA to access CA–CIAM surface than the AA–CIAM and CA–CNAM. The nature of the carboxylic acid (AA, MAA, CA) significantly affected not only the morphology of the prepared membrane (Fig. 4b to Fig. 4d), but also the adsorption performance. The data also showed that the imprinted membrane significantly adsorbed more GA than the non-imprinted membrane for either functional monomer, which might be ascribed to more cavities or adsorption sites obtained on the surface of imprinted membrane.

The effect of RTIL and the amount of polymer layer on the imprinted membranes were expected to strongly affect the adsorption of GA. Fig. 8 shows the GA adsorption on the membranes (CA–CIAM0, CA–CIAM1, CA–CIAM2, and CA–CIAM3) coated with various amounts of imprinted polymer. The adsorption capacity of GA at equilibrium for CA–CIAM1 (143.6×10^{-3} μmol g^{-1}) was much higher than that of CA–CIAM0 (86.77×10^{-3} μmol g^{-1}). It could be ascribed to that when no RTIL was involved, the imprinted layer on the membrane was less porous, which was responsible for the poor recognition ability, since less porosity led to less chances for the analyte to access the recognition site.

Comparing with CA–CIAM1, CA–CAM2 and CA–CIAM3, the amount of GA adsorption increased with the increase in the amount of coated polymer due to more adsorption sites on the surface of CA–CIAM. However, the increasing trend was not very obvious, which might be ascribed to that excessive polymer on the surface limited the effect on the specific adsorption of GA. With the increase in the amount of polymer, less porous on the membrane reduced efficient recognition sites.

3.6. Permeability

3.6.1 Permselectivity of composite imprinted membranes

In the permeation experiment, the permeation concentrations of SA and GA through different membranes at the feed mixture concentration of 0.35 mmol L^{-1} in 3 h were shown in Fig. 9. In order to study the effect of the content of polymerization layer on the permeability performances, Fig. 9a shows the time-dependent permeation curves of SA and GA on the blank Al_2O_3 ceramic membrane and the CA–CIAM(1,2,3), respectively. As shown in Fig. 9a, compared with the Al_2O_3 ceramic membrane, the concentration of SA in the receiving chamber was much higher than that of GA for the three CA–CIAMs, indicating that the three CA–CIAMs had a special selectivity of GA. Comparing the three CA–CIAMs, it was also found that the diffusion rate of both SA and GA through CA–CIAM3 was much lower than other two imprinted membranes (CA–CIAM1 and CA–CIAM2). Moreover, it can be clearly seen that the CA–CIAM2 shows the greatest differences in the concentration between SA and GA in the receiving chamber among the three CA–CIAMs, indicating that the CA–CIAM2 has better separation effect for SA and GA. It may suggest that

CA–CIAM1 with little polymer on the Al_2O_3 ceramic membrane has limit recognition sites, while excessive polymer will increase non specific adsorption and decrease the permeation rate of competing molecule, which affected the separation effect.

Fig. 9b also shows the time-dependent permeation curves of the CA–CIAM0, CA–CIAM2, CNAM, respectively. Compared to imprinted membranes, the diffusion rate of SA through the CNAM was closed to that of GA. This means that the non-imprinted membrane exhibited non specific adsorption to SA and GA. Comparing CA–CIAM0 and CA–CIAM2, it was also clearly found that both the diffusion rate of SA and GA through CA–CIAM0 were much lower than that of CA–CIAM2. Especially, CA–CIAM2 exhibited excellent separation effect for SA and GA compared with CA–CIAM0. It can be attributed to the CA–CIAM0 with no RTIL involved was less porous, which caused the blocking permeation of SA and GA through the imprinted membranes. And there were less efficient recognition sites, which will affect the separation effect. So RTIL incorporated will play an important role in the separation process for imprinted membrane.

3.6.2 Mass transfer performance

According to the mentioned above, the imprinted membrane itself is of high importance in success of the membrane separation. The inherent nature of the polymer membranes is their specific recognition properties. From permeation experiments, the permeability coefficients of SA and GA through different imprinted membranes were calculated by equation 6 as shown in Table 3. The results show that the Al_2O_3 membrane has a similar permeability coefficients for both SA (3.736×10^{-4} cm^2 s^{-1}) and

GA (3.841×10^{-4} cm^2 s^{-1}) compared to the imprinted and non-imprinted membrane, indicating that Al_2O_3 membrane shows almost the same mass transfer ability during the permeation process. Moreover, as for the imprinted membranes (CA–CIAM0, CA–CIAM1, CA–CIAM2, CA–CIAM3), all the *P* values of SA is much higher than GA. This suggests that GA has a much stronger interaction with imprinted membranes and diffuses faster than SA. Because the SA molecules compete with GA molecules to go through the inner pores of the imprinted layer, GA as template can bind with the group on the imprinted membrane more powerfully and then SA will get through the composite membrane preferentially. Thus, the imprinted membrane has a special selectivity to GA. Additionally, the CA–CIAM2 shows a higher selectivity than that of other imprinted membranes and CA–CNAM2 according to the results of the values separation factors ($\alpha_{SA/GA}$) summarized in Table 3, which was agreed with the earlier report by Jiro Komiyama et al.[30-31]

The following equation was used to compute the overall mass transfer coefficient (K_{ov}) using concentration as the driving force [32]:

$$\left(\frac{K_{OV}A}{V_F}\right)t = \frac{1}{1+\phi}\ln\left(\frac{C_{F,0}}{(1+\phi)C_F - \phi C_{F,0}}\right) \quad (9)$$

where $\phi = \frac{V_F}{V_R}$

The right hand side of equation is plotted against time to estimate K_{OV}. This plot yields a linear curve with the slope ($K_{OV}A/V_R$) containing K_{OV}. The values of K_{OV} can be determined from a plot of $C_{F,0}$ against *t* using nonlinear regression analysis.

As shown in Table 3, the experimental data were well fitted by the model for varied

membrane with high R^2 values. Fig. 10 shows the experimental points and nonlinear predicted points according to the parameters of the mass transfer model in Table 3. Apparently, the nonlinear model provided fine fitting of SA and GA for various membranes in Fig 10a and b.

In Table 3, the experimentally determined mass transfer coefficients of SA was close to that of GA for Al_2O_3 membrane, while the *K*ov values of SA were much higher than that of GA for CA–CIAM1, CA–CIAM2 and CA–CIAM3, respectively. However, both the mass transfer coefficients of SA and GA for CA–CIAM3 were lower than that of CA–CIAM1 and CA–CIAM2, These means that the imprinted layer can greatly affect the mass transfer ability of the Al_2O_3 ceramic membrane.

Additionally, the mass transfer coefficients of SA for CA–CIAM2, CA–CIAM0 and CNAM2 were 5.667×10^{-3}, 2.668×10^{-3}, 5.330×10^{-3} cm s^{-1}, respectively, while the mass transfer coefficients of GA for the three membranes were 1.120×10^{-3}, 1.009×10^{-3}, 3.001×10^{-3} cm s^{-1}. Among the three membranes, CA–CIAM2 has a high mass transfer coefficients of SA and low mass transfer coefficients of GA, showing a favorable separation effect of SA and GA. The inverse of the mass transfer coefficient is the mass transfer resistance. Compared with the CA–CNAM2, CA–CIAM2 has the smallest mass transfer coefficient for GA, suggesting the CA–CIAM2 has maximum resistance for transferring GA.

In the mass transfer process, analyte transport takes place from the feed solution to the receiving solution. In our research, since the solvents in both reservoirs are the same, the liquid resistances are greatly reduced. Additionally, our aim was to obtain

the separation of SA and GA by forming different mass transfer rate via the interaction between the analytes and the imprinted layer on the Al_2O_3 membrane. On the basis of Table 3, different membranes show different overall mass transfer coefficients for both SA and GA. So the resistances of the liquid films can be negligible compared to those of the membrane. It may conclude that the mass transfer across the membrane phase is the rate-controlling step. This general assumption is consistent with the reported literature.[33]

3.7. Selective permeation mechanism

The permeability experiments mentioned above showed that the imprinted membranes showed higher diffusion rate for the completing molecule (SA) than for the template (GA). So the major mechanisms applied in analyzing the selective transport can be regarded retarded permeation, which was due to affinity binding–faster transport of SA, until a saturation of recognition sites with GA is reached.[34] The transport of the target analytes go across the membrane by adsorbing on and desorbing from the imprinted skin on the Al_2O_3 membrane. In the permeation experiment, the template molecule (GA) can preferentially bond with the functional groups in the recognizing sites on the imprinted membrane. Meanwhile, the SA molecules can't match the recognition cavity well in size and shape. So, the imprinted membrane had hardly recognition effect for non-template and SA molecules can be easily desorbed from the membrane. As a result, SA had more chance to transfer continuously from one side to the other side of the composite membrane. So, the imprinted membrane acted as an adsorptive membrane.[35] Therefore, such transport

mechanism for permeation of the SA and GA towards the imprinted Al_2O_3 membrane was accordance with the retarded mechanism mentioned above.

3.8. Design of RSM for optimization of dynamic separation

A numerical optimization combined with a desirability function was applied to calculate the optimum values of the concentration of GA (mmol L^{-1}), the temperature (^oC) and the flow rates (mL min^{-1}) to provide more theoretical basis in the dynamic separation process. For industrial application, a dynamic separation study is essential for continuous flow systems. The optimization step of proposed method was carried out using a Box–Behnken design (BBD). In this research, CA–CIAM2 was selected to study the dynamic separation of GA and SA.

3.8.1 Statistical analysis and the model fitting

There were a total of 17 runs with different combinations of the physical parameters for optimizing the three individual parameters in the BBD. The experimental conditions and the selective separation factors of GA and SA according to the factorial design were shown in Table 2. The goal of the optimization was to maximize the separation factors. Results also showed that the response values (β) ranged from 0.837 to 13.01. The results of this limited number of experiments provided a statistical model that was used to identify trends in high separation factor for the dynamic separation process. Table 2 shows the matrix and the separation factors (β). The quadratic models below illustrate the relationship of the three variables and Y (β).

$$Y=2.13-4.26A-0.37B-1.40C+0.30AB+1.16AC+0.16BC+3.50A^2-0.026B^2+0.14C^2$$

The analyses of variance (ANOVA) results for the response surface quadratic model

are shown in Table 4. The *p*-value was used to check the significance of each coefficient, and the smaller the *p*-value was, the more significant the corresponding coefficient was. The ANOVA of the quadratic regression models demonstrated the models to be significant with low probability ($p < 0.0001$). The predicted versus observed values of the separation factors indicated good agreement between the polynomial regression model and the experimental data, with the coefficient of determination (R^2) of 0.9879. The lack of fit measures the failure of the model to represent data in the experimental domain at points which are not included in the regression. The non-significant value of lack of fit (>0.05) revealed that the quadratic model is statistically significant for the response (β).

The contribution of each parameter/factor (first and second order) besides the interaction between them on the separation effect was shown in Table 4. All coefficients with *p*-values less than 0.05 are significant. As seen in Table 4, the analyses indicated that A, C, AC, A^2 are significant model terms for separation of GA from SA, while the other term coefficients (B, AB, BC, B^2 C^2) were not significant ($p > 0.05$).

3.8.2 Response surface plots and response optimization

Response surface methodology was used to determine the optimal response for the separation of GA from SA. The results of separation factors affected by concentration of GA, flow rate and temperature are presented in Fig. 11. Three-dimensional (3D) surface plots showed visually the effects and interaction of two independent variables on the responding variable as third independent variable

was kept at level zero.

Fig. 11a giving the separation factor between GA and SA as a function of concentration and flow rate at fixed temperature (30.0 ^{o}C), indicated that the separation factor rapidly increased with the decrease of the concentration of GA from 0.325 to 0.0325 mmol L^{-1} and decreased with the increase of the flow rate from 1.0 to 5.0 mL min^{-1}. It could be explained a decrease in the residence time, which restricted the contact of GA and SA mixed solution to the CA–CIAM. At higher flow rate, the GA did not have enough time to diffuse into the binding sites on CA–CIAM and they passed the membrane fast before equilibrium occurred. Moreover, the increase of the separation factor when the concentration of GA in the mixture of GA and SA decreased could be related with the chemical environment, the binding sites preservation of the CA–CIAM. The number of effective binding sites was limited after imprinting on the membrane. So it suggested that the imprinted membrane favored the separation of the mixture containing lower GA initial concentrations.

At the meanwhile, Fig. 11b shows the 3-D response surface plot at varying temperature and concentration at fixed flow rates of 3.0 mL min^{-1}. The maximum separation factor can be achieved when temperature and concentration of GA at 15.0 ^{o}C and 0.0325 mmol L^{-1}. At high temperatures, less GA molecules were required to satisfy the maximum adsorption capacity of the CA–CAIM. Therefore, the low temperature favors the separation effect of GA from SA, indicating an exothermic process.

Fig. 11c shows the 3-D response surface plot with varying temperature and flow

rates at fixed concentration of GA of 0.179 mmol L^{-1}. The maximum separation factor can be achieved in the case of temperature and flow rate at the value of 15.0 ^{o}C and 1.0 mL min^{-1}, respectively. The results are consitent with the discussion mentioned above.

3.8.3 Optimization and verification of the model

According to Fig. 10a-c, it can be concluded that the optimal conditions giving the maximum response for selectivity coefficient (13.39) was found in conditions of A = 0.0325 mmol L^{-1}, B = 15 ^{o}C, C = 1.0 mL min^{-1}.

For their validation of the optimum conditions, triplicate confirmatory experiments were carried out under the optimized conditions and the average separation factor (β) was 13.26 ± 0.87%. The results are closely related with the data obtained from optimization analysis, indicating Box–Behnken design could be effectively used to optimize the separation GA from SA.

4. Conclusions

A novel composite imprinted alumina membrane (CIAM) was successfully prepared via the RTIL-mediated NHSG methodology for selective separation of GA from SA. The adsorption capacity, flux and permeation selectivity of the imprinted membranes depended on the functional monomers and the crosslinking degree of polymer layer on the alumina membrane. CA–CIAM2 was found to be the promising imprinted membrane to increase the effect on separating GA from SA. Additionally, incorporation of RTIL can greatly increase the porosity, flux and recognition ability, and further improve the selectivity of the CIAM to GA.

RSM was used to estimate and optimize the experimental variables (the concentration of GA, temperature and flow rate) in the dynamic separation process. Under the optimal conditions of GA concentration at 0.0325 mmol L^{-1}, temperature at 15.0 ^{o}C, flow rate at 1.0 mL min^{-1}, the experimental selectivity factor was 13.26 ± 0.87%, which was close to the predicted selectivity factor value. We expect that the RTIL-mediated NHSG protocol is promising as a general strategy for the fabrication of high selective imprinted membrane for purification of trace analytes in the complex matrix.

Acknowledgments

This work was financially supported by the National Natural Science Foundation of China (Nos. 21077046, 21107037, 21176107, 21174057, 2100403, 21207051), National key basic research development program (973 Program, No. 2012CBB21500), Ph.D. Programs Foundation of Ministry of Education of China (No. 20123227120015) and Natural Science Foundation of Jiangsu Province (BK2011461, SBK2011459, BK2011514). China Postdoctoral Science Foundation funded project (Nos. 2012M511220, 2013M530240).

References

1 N. H. Ullsten, M. Gällstedt, E. Johansson, A. Gräslund and M. S. Hedenqvist, *Biomacromolecules*, 2006, **7**, 771.

2 M. Hussain, A. Javeed, M. Ashraf, Y. Zhao, M. M. Mukhtar and M. Ur Rehman, *Int. Immunopharmacol.*, 2012, **12**, 10.

3 A. L. Ahmad, M. R. Othman and H. Mukhtar, *Int. J.Hydrogen Energy.*, 2004, **29**, 817.

4 H. M. Zhang, X. Quan, S. Chen and H. M. Zhao, *Environ. Sci. Technol*., 2006, **40**, 6104.

5 N. Hilal, V. Kochkodan, G. Busca, O. Kochkodan and B. P. Atkin, *Sep. Purif. Technol*., 2003, **31**, 281.

6 T. A. Sergeyeva, O. O. Brovko, E. V. Piletska, S. A. Piletsky, L. A. Goncharova, L. V. Karabanova, L. M. Sergeyeva and A. V. El'skaya, *Anal. Chim. Acta*, 2007, **582**, 311.

7 M. S. da Silva, R. Viveiros, A. Aguiar-Ricardo, V. D.B. Bonifácio and T. Casimiro, *RSC Advances*, 2012, **2**, 5075.

8 C.Y. He, Y. Y. Long, J. L. Pan, K. Li and F. Liu, *J. Biochem. Biophys. Methods*, 2007, **70**, 133.

9 Z. Zhang, M. Zhang, Y. Liu, X. Yang, L. Luo and S. Yao, *Sep. Purif. Technol.*, 2012, **87**, 142.

10 R. J. Ansell, J. K. Kuah, D. Wang, C. E. Jackson, K. D. Bartle and A. A. Clifford, *J. Chromatogr. A*, 2012, **1264**, 117.

11 G. Zhu, J. Fan, Y. Gao, X. Gao and J. Wang, *Talanta*, 2011, **84**, 1124.

12 H. Henschel, N. Kirsch, J. Hedin-Dahlström, M. J. Whitcombe, S. Wikman and I. A. Nicholls, *J. Mol. Catal B-Enzym.*, 2011, **72**, 199.

13 C. Baggiani, F. Biagioli, L. Anfossi, C. Giovannoli, C. Passini and G. Giraudi, *React. Funct. Polym.*, 2013, **73**, 833.

14 J. L. Urraca, M. D. Marazuela, E. R. Merino, G. Orellana and M. C. Moreno-Bondi, *J. Chromatogr. A*, 2006, **1116**, 127.

15 A. Higuchi, M. Tamai, Y. Ko, Y. Tagawa, Y. Wu, B. Freeman, J. Bing, Y. Chang and Q. Ling, *Polym. Rev.*, 2010, **50**, 113.

16 M. E. Díaz-García and R.B. Laíño, *Microchim. Acta*, 2005, **149**, 19.

17 S. Fireman-Shoresh, I. Popov, D. Avnir and S. Marx, *J. Am. Chem. Soc.*, 2005, **127**, 2650.

18 Z. Jiang, Y. Yu and H. Wu, *J. Membr. Sci.*, 2006, **280**, 876.

19 H. F. Wang, Y. Z. Zhu, X. P. Yan, R. Y. Gao and J. Y. Zheng, *Adv. Mater.*, 2006, **18**, 3266.

20 S. Panja, P. K. Mohapatra, S. C. Tripathi, P. M. Gandhi and P. Janardan, *Sep. Purif. Technol*., 2012, **96**, 289.

21 T. Welton, *Coord. Chem. Rev.*, 2004, **248**, 2459.

22 P. Hapiot and C. Lagrost, *Chem. Rev*., 2008, **108**, 2238.

23 Y. Zhou, J. H. Schattka and M. Antonietti, *Nano Lett.*, 2004, **4**, 477.

24 Y. Zhou and M. Antonietti, *Chem. Mater.*, 2004, **16**, 544.

25 Y. Liu, M. Wang, Z. Li, H. Liu, P. He and J. Li, *Langmuir*, 2005, **21**, 1618.

26 J. G. Huddleston, H. D. Willauer, R. P. Swatloski, A. E. Visser and R. D. Rogers,

Chem. Commun., 1998, 1765.

27 G. E. P. Box and K. B. Wilson, *J. R. Stat. Soc. B*, 1951, **13**, 1.

28 J. Han, Y. Wang, Y. Liu, Y. F. Li, Y. Lu, Y. S. Yan, L. Ni, *Anal. Bioanal. Chem.*, 2013, **405**, 1245.

29 J. F. He, Q. H. Zhu and Q. Y. Deng, *Spectrochim. Acta A*, 2007, **67**, 1297.

30 Z. Y. Jiang, Y. X. Yu and H. Wu, *J. Membr. Sci.*, 2006, **280**, 876–882.

31 K. Taki, I. Arita, M. Satoh and J. Komiyama, *J. Polym. Sci. Pol. Phys.*, 1999, **37**, 1035.

32 R. Valadez-Blanco and A. G. Livingston, *J. Membr. Sci.*, 2009, **326**, 332.

33 M. Dingemans, J. Dewulf, L. Braeckman, H. V. Langenhove, K. Friess, V. Hynek and M. Sipek, *J. Membr. Sci*., 2008, **322**, 234.

34 M. Ulbricht, *J. Chromatogr. B*, 2004, **804**, 113.

35 D. Keith Roper and E. N. Lightfoot, *J. Chromatogr. A*, 1995, **702**, 3.

Table 1
Protocol of prepolymerization solutions[a]

Membranes	SA (mmol)	Carboxylic Acid[b]	MPS (mmol)	RTIL (mL)	AIBN (mmol)
AA-CIAM	1	AA	8	2	0.12
AA-CNAM	0	AA	8	2	0.12
MAA-CIAM	1	MAA	8	2	0.12
MAA-CNAM	0	MAA	8	2	0.12
CA-CIAM1	1	CA	4	2	0.09
CA-CIAM2	1	CA	8	2	0.12
CA-CNAM2	0	CA	8	2	0.12
CA-CIAM3	1	CA	16	2	0.2
CA-CIAM0	1	CA	8	0	0.12

[a]ACN was added to ensure a total volume of 12 mL.

[b]The amount of three carboxylic acid(AA, MAA and CA) are the same 4 mmol according to the results in Fig.1

Table 2

BBD experiment design and result for the optimization of the separation factors between SA and GA.

Run	*A* (*C*: mmol L^{-1})	*B* (T: ^{o}C)	*C* (*V*: mL min^{-1})	β
1	0.0325	45.0	3.0	8.890
2	0.325	30.0	1.0	2.123
3	0.0325	30.0	1.0	13.01
4	0.325	15.0	3.0	1.712
5	0.179	15.0	5.0	1.179
6	0.179	15.0	1.0	3.495
7	0.179	30.0	3.0	2.018
8	0.325	45.0	3.0	1.023
9	0.179	30.0	3.0	1.512
10	0.179	30.0	3.0	2.101
11	0.179	45.0	5.0	1.312
12	0.179	30.0	3.0	2.301
13	0.179	45.0	1.0	2.971
14	0.179	30.0	3.0	2.716
15	0.0325	15.0	3.0	10.78
16	0.325	30.0	5.0	0.837
17	0.0325	30.0	5.0	7.081

Table 3

Experimental permeability results for SA and GA through the various imprinted membranes.

Membranes	Substrate	$J\times10^{-7}$ (mmol cm^{-2} s^{-1})	$P\times10^{-4}$ (cm^2 s^{-1})	$\alpha_{SA/GA}$	Mass transfer model	
					$K_{ov}\times10^{-3}$ (cm s^{-1})	R^2
Al_2O_3 membrane	SA	6.537	3.736	0.9723	8.681	0.9700
	GA	6.723	3.841		7.001	0.9733
CA-CIAM1	SA	8.995	5.140	1.924	7.329	0.9809
	GA	4.675	2.671		1.953	0.9758
CA-CIAM2	SA	8.447	4.827	2.693	5.667	0.9880
	GA	3.136	1.792		1.120	0.9868
CA-CIAM3	SA	6.409	3.662	2.062	3.012	0.9955
	GA	3.107	1.775		1.099	0.9907
CA-CIAM0	SA	6.033	3.448	2.083	2.668	0.9957
	GA	2.897	1.655		1.009	0.9931
CA-CNAM	SA	8.098	4.628	1.303	5.330	0.9967
	GA	6.214	3.551		3.001	0.9942

Table 4

Estimated regression model of relationship between response variables (β) and independent variables (A, B, C).

Factor	SS	df	MS	F	p	
Model	219.7	9	24.42	63.67	< 0.0001	significant
A	145.1	1	145.05	378.29	< 0.0001	
B	1.100	1	1.10	2.88	0.1338	
C	15.65	1	15.65	40.83	0.0004	
AB	0.360	1	0.36	0.94	0.3644	
AC	5.390	1	5.39	14.06	0.0072	
BC	0.110	1	0.11	0.28	0.6122	
A^2	51.51	1	51.51	134.33	< 0.0001	
B^2	2.776×10^{-3}	1	2.776×10^{-3}	7.239×10^{-3}	0.9346	
C^2	0.077	1	0.077	0.20	0.6669	
Lack of Fit	4.63	3	1.54	6.36	0.0530	not significant

Figure caption

Fig. 1. Adsorption spectra of the GA in the presence of various concentrations of functional monomers (MAA (a), AA(b), CA (c)) in acetonitrile. Concentration of GA: 0.1mmol L^{-1}, corresponding pure functional monomer solutions as blanks.

Fig. 2. FTIR spectrum of [BMIM]Cl and [BMIM]BF_6.

Fig. 3. AFM topographical images revealing changes in the surface of ceramic membrane: Al_2O_3 ceramic membrane (a: two dimension, b: three-dimension), CA–CIAM (c: two dimension, d: three-dimension).

Fig. 4. SEM images of (a) Al_2O_3 ceramic membrane, (b) MAA–CIAM, (c) AA–CIAM, (d) CA–CIAM1, (e) CA–CIAM2, (f) CA–CIAM3 and the inset shows an enlargement of part of the four images, respectively.

Fig. 5. SEM images of cross section of the studied membranes (a–d): (a) original membrane, (b) CA–CIAM0, (c) CA–CIAM2, (d) CA–CNAM2.

Fig. 6. The flux of GA aqueous solution through different membranes.

Fig. 7. Batch adsorption of GA by CIAM and CNAM prepared with AA, MAA and CA as functional monomers, respectively.

Fig. 8. Batch adsorption of GA by varied imprinted membrane.

Fig. 9. Time-permeation curves of SA and GA through the various membranes (Feed concentration = 0.360 mmol L^{-1}).

Fig. 10. Non-linear regression of mass transfer model for SA and GA through different membranes.

Fig. 11. Response surfaces plots for selective factors as a function of **a**: concentration of GA and flow rate, **b**: concentration of GA and temperature, **c**: flow rate and temperature.

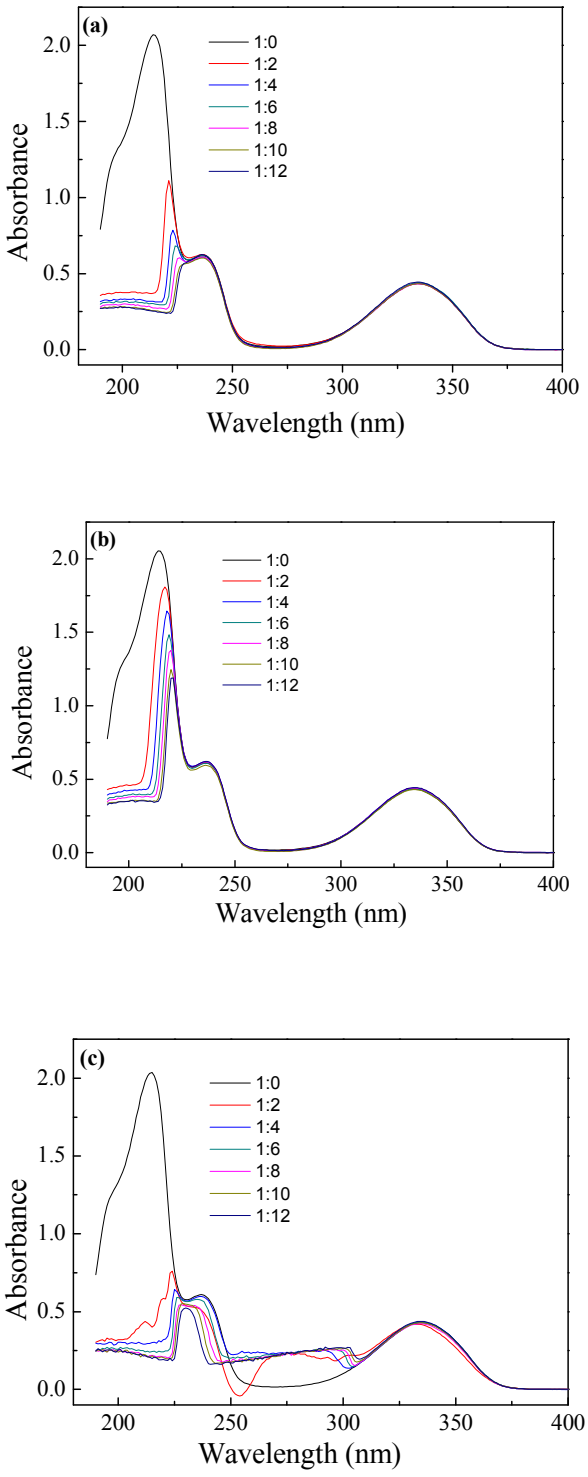

Fig. 1.

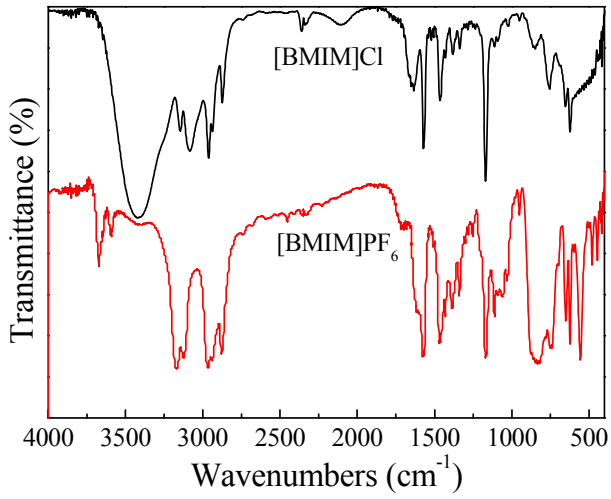

Fig. 2.

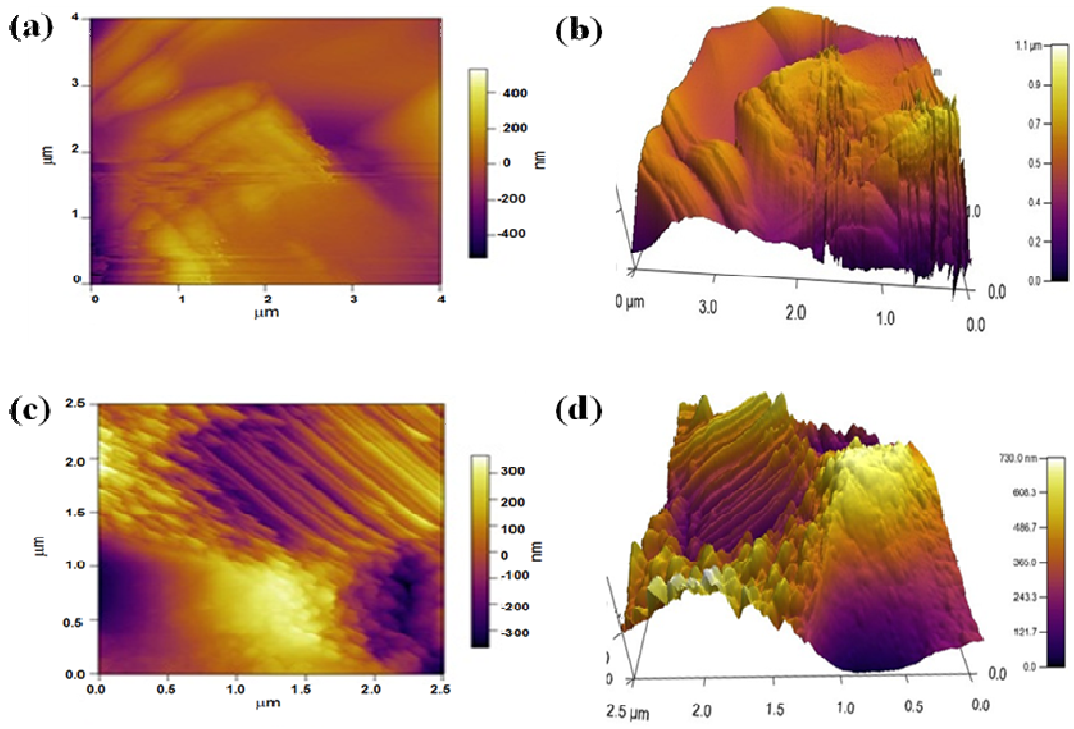

Fig. 3.

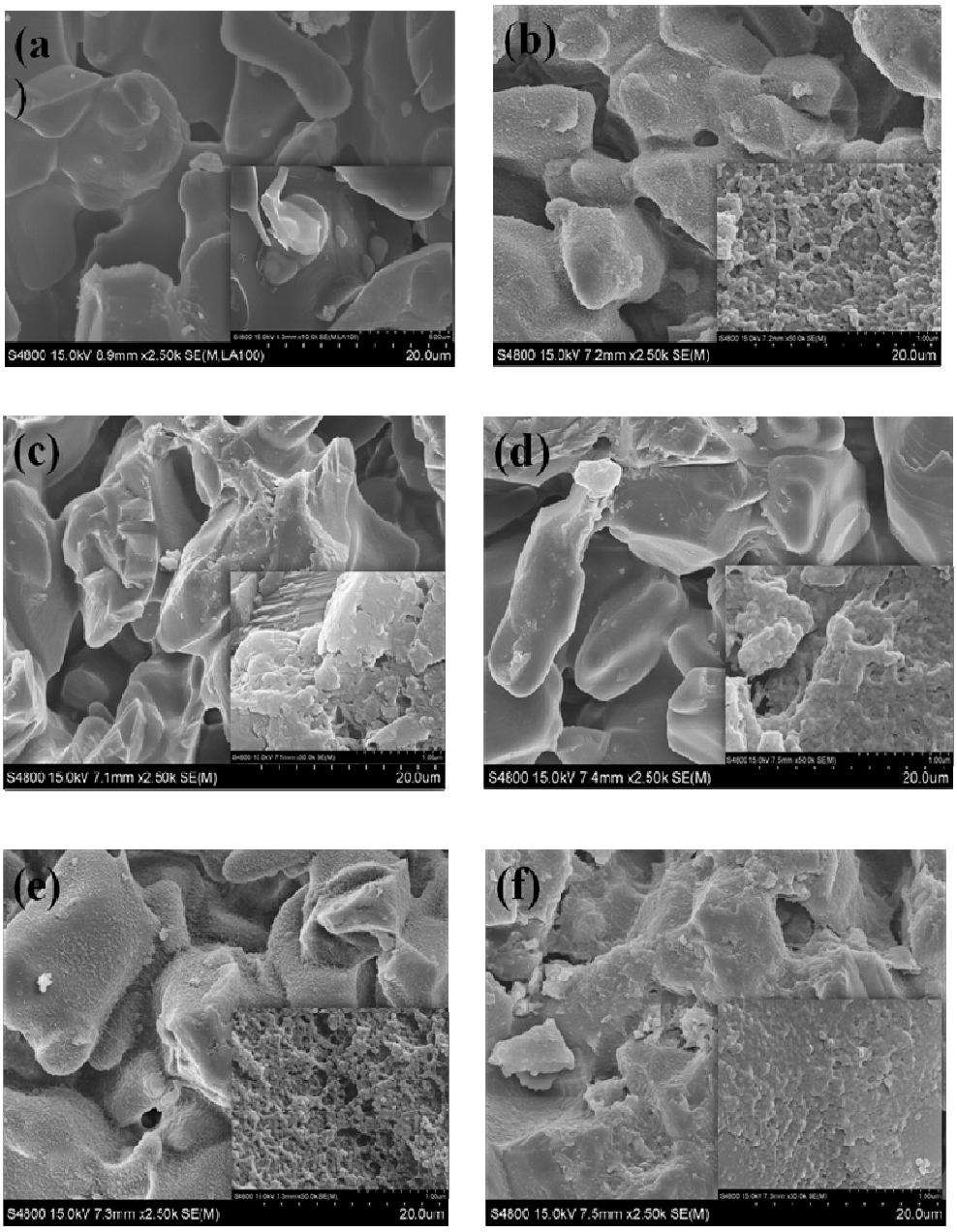

Fig. 4.

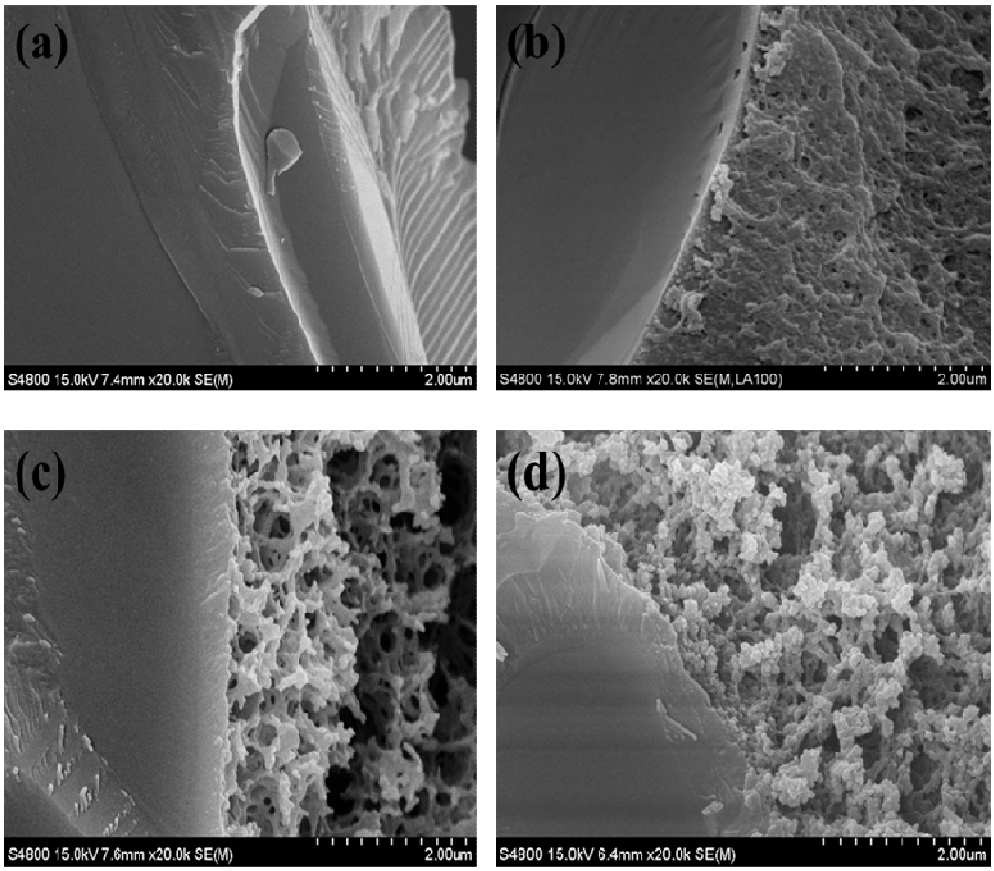

Fig. 5.

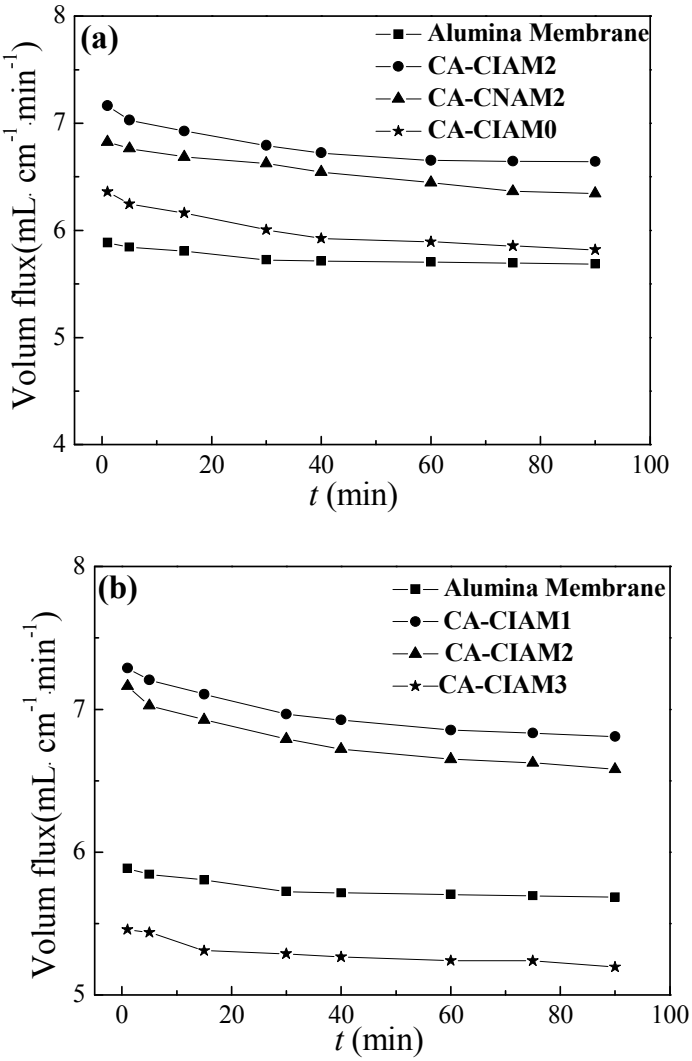

Fig. 6.

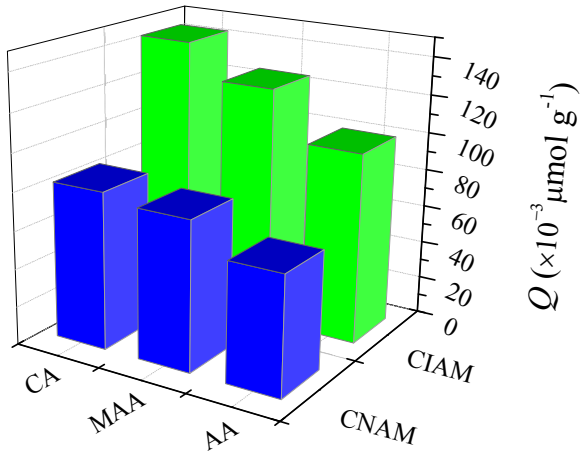

Fig. 7.

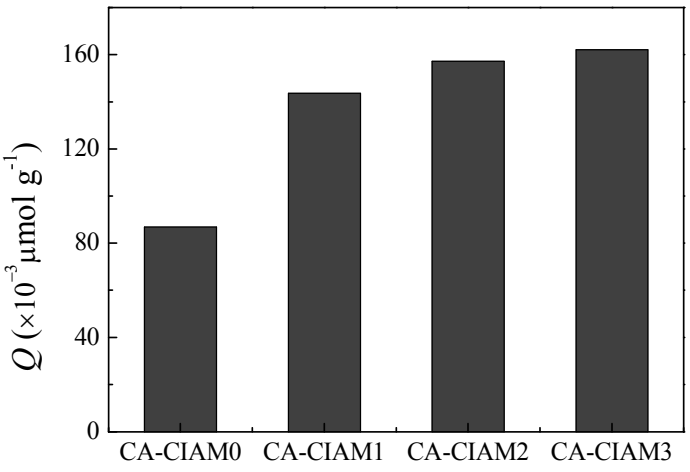

Fig. 8.

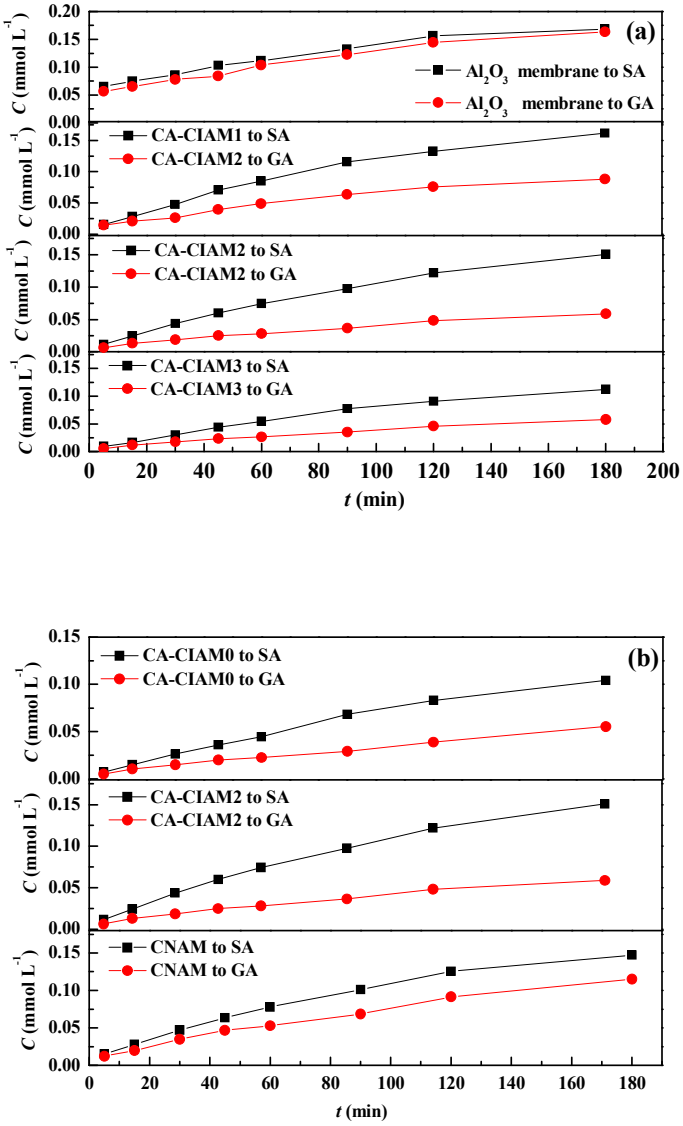

Fig. 9.

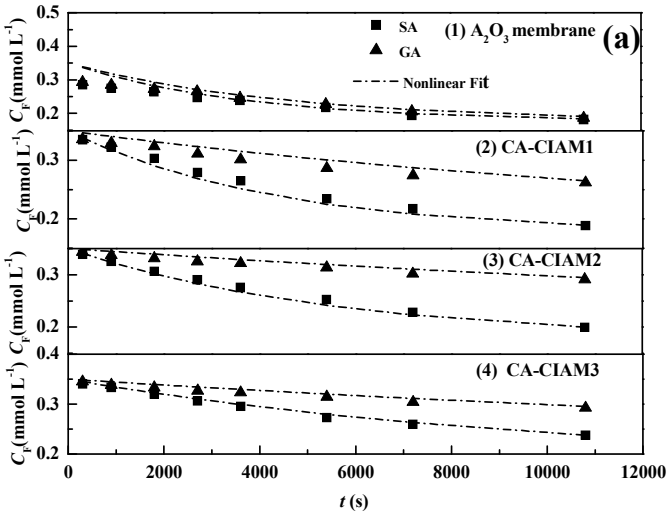

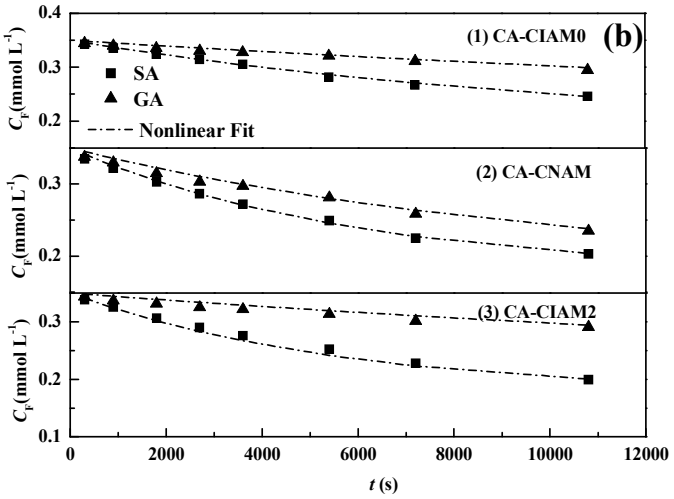

Fig. 10.

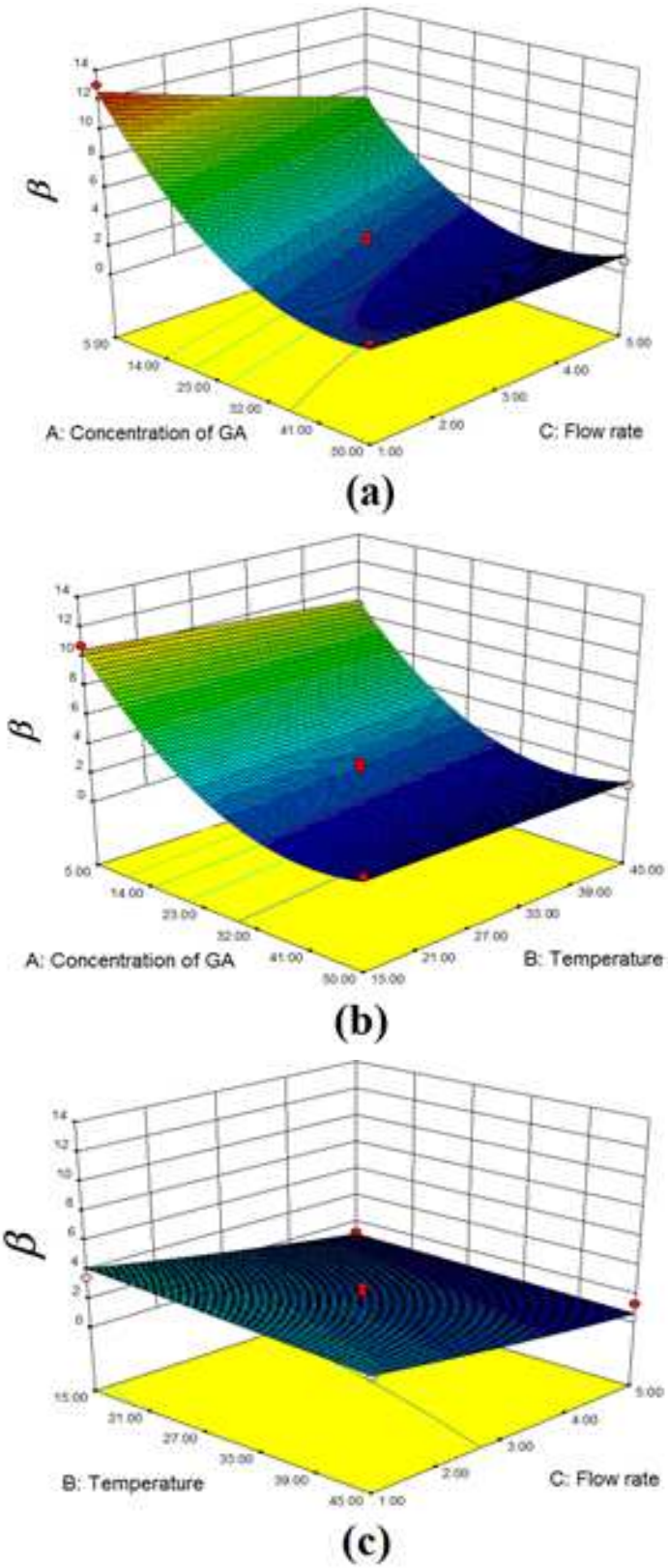

Fig. 11.

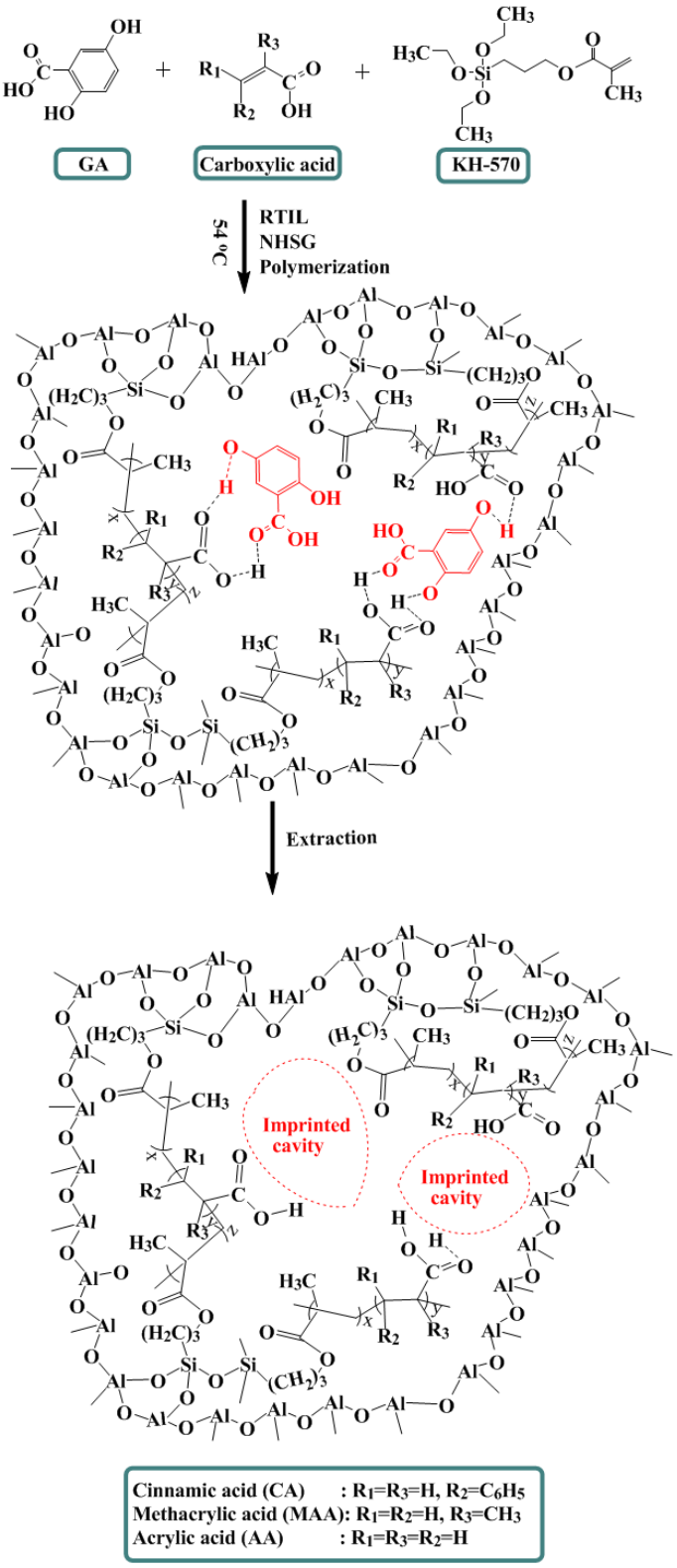

Scheme 1. Scheme and possible mechanism of the RTIL mediated NHSG route to prepare the composite imprinted alumina membrane.